NUMERICAL SIMULATION OF ELASTIC WAVE SCATTERING FROM THREE-DIMENSIONAL AXISYMMETRIC SURFACE FEATURES

Peter H Albach and Leonard J Bond

NDE Centre
Department of Mechanical Engineering
University College London
Torrington Place
London WC1E 7JE
United Kingdom

INTRODUCTION

Due to more intensive use of civil and military aircraft there are growing demands for accurate and reliable methods in non-destructive testing. One of the areas receiving specific attention is the detection and characterisation of corrosion [1]. The study presented here is concerned with the scattering of ultrasound waves from an isolated corrosion pit on the remote side of a thick aluminium plate. The corrosion pit is represented by a three-dimensional hemispherical surface indentation of radius a in an elastic half-space, and the wave field generated by an ultrasonic transducer is assumed to be a time harmonic plane wave incident on to the surface feature at an arbitrary angle, see Fig. 1. The scattering problem is solved by means of a boundary method, and the surface displacements in the vicinity of the scatterer and the scattered far-field components are represented for compressional waves incident at 60 degrees and shear waves normally incident on to the surface obstacle. The diameter of the surface indentation can vary between the fraction of a wavelength and two wavelengths. The results shown here were calculated for $2a / \lambda = 0.5$ and 1.0.

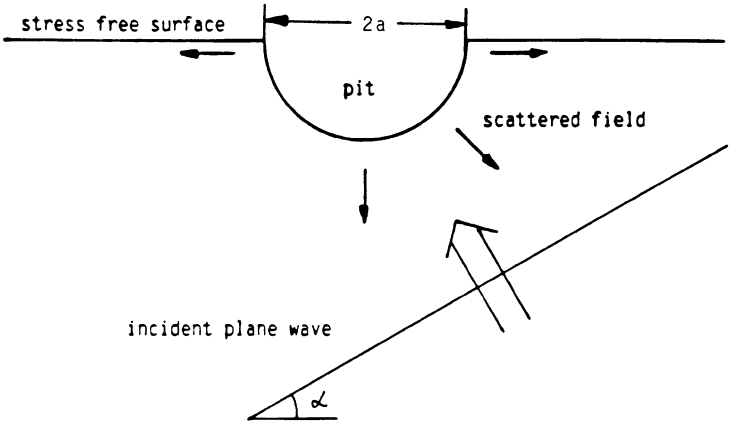

Fig.1 . Time harmonic plane wave incident at angle α on to a hemispherical surface indentation in a half-space

Review of Progress in Quantitative Nondestructive Evaluation, Vol. 9
Edited by D.O. Thompson and D.E. Chimenti
Plenum Press, New York, 1990

MATHEMATICAL METHOD

The boundary method employed here originates in geophysics [2], where it is used to simulate movements of the earth's crust under the influence of earthquakes waves. The incident and reflected plane waves in an unperturbed half space are expanded in terms of spherical vector functions [3], and the scattered wave field due to the surface disturbance is superimposed as a series of spherical vector functions with unknown coefficients. These coefficients are determined by imposing the boundary conditions - vanishing normal stress components along the perturbed surface - via a least squares matching method [4].

The time harmonic elastic wave equation can be written as

$$(\lambda + 2\mu)\ \text{grad div}\ \vec{u} - \mu\ \text{curl curl}\ \vec{u} + \rho\ \omega^2\ \vec{u} = 0 \tag{1}$$

Employing the Helmholtz theorem

$$\vec{u} = \text{grad}\ \varphi + \text{curl}\ \vec{A} \tag{2a}$$

$$\text{div}\ \vec{A} = 0 \tag{2b}$$

leads to two separate wave equations:

- scalar wave equation

$$\nabla^2 \varphi + k_p^2\ \varphi = 0 \tag{3a}$$

$$k_p^2 = \frac{\omega^2\ \rho}{\lambda + 2\mu} \tag{3b}$$

- vector wave equation

$$\nabla^2 \vec{A} + k_s^2\ \vec{A} = 0 \tag{4a}$$

$$k_s^2 = \frac{\omega^2\ \rho}{\mu} \tag{4b}$$

where the scalar wave equation describes compressional wave motion and the vector wave equation describes shear wave motion. In spherical coordinates it is possible to split the vector potential under restriction (2b) into two scalar potentials, both solutions to the scalar wave equation [3]

$$\nabla^2 \psi + k_s^2\ \psi = 0 \tag{5a}$$

$$\nabla^2 \chi + k_s^2\ \chi = 0 \tag{5b}$$

Now equation (2a) can be written as

$$\vec{u} = \vec{L}\ (k_p, r, \theta, \phi) + \vec{M}\ (k_s, r, \theta, \phi) + \vec{N}\ (k_s, r, \theta, \phi) \tag{6}$$

where $\vec{L}$, $\vec{M}$ and $\vec{N}$ are the so-called Hansen vectors defined as

$$\vec{L}\ (k_p, r, \theta, \phi) = \text{grad}\ \varphi\ (k_p, r, \theta, \phi) \tag{7}$$

$$\vec{M}\ (k_s, r, \theta, \phi) = \text{curl}\ (r\ \psi\ (k_s, r, \theta, \phi)\ \vec{e}_r) \tag{8a}$$

$$= \text{grad}\ (r\ \psi) \times \vec{e}_r \tag{8b}$$

$$\vec{N}\ (k_s, r, \theta, \phi) = \tfrac{1}{k_s}\ \text{curl curl}\ (r\ \chi\ (k_s, r, \theta, \phi)\ \vec{e}_r) \tag{9a}$$

$$= \tfrac{1}{k_s}\ \text{grad}\ \frac{\partial (r\ \chi)}{\partial r} + k_s\ r\ \chi\ \vec{e}_r \tag{9b}$$

with $\vec{e}_r$ denoting the unit vector in radical direction

The scalar potentials φ, ψ and χ are solutions to the scalar wave equation in spherical coordinates. It is therefore possible to write the potentials as an infinite series

$$\varphi(k_p, r, \theta, \phi) = \sum_{n=0}^{\infty} \sum_{m=0}^{n} \sum_{\sigma=e}^{o} a_{\sigma,m,n} V_{\sigma,m,n}(k_p, r, \theta, \phi) \quad (10a)$$

$$\psi(k_s, r, \theta, \phi) = \sum_{n=0}^{\infty} \sum_{m=0}^{n} \sum_{\sigma=e}^{o} b_{\sigma,m,n} V_{\sigma,m,n}(k_s, r, \theta, \phi) \quad (10b)$$

$$\chi(k_s, r, \theta, \phi) = \sum_{n=0}^{\infty} \sum_{m=0}^{n} \sum_{\sigma=e}^{o} c_{\sigma,m,n} V_{\sigma,m,n}(k_s, r, \theta, \phi) \quad (10c)$$

$$V_{e,m,n}(k, r, \theta, \phi) = z_n(kr) P_n^m(\cos\theta) \cos(m\phi) \quad (11a)$$

$$V_{o,m,n}(k, r, \theta, \phi) = z_n(kr) P_n^m(\cos\theta) \sin(m\phi) \quad (11b)$$

with the following meaning for the subscripts:

'σ' : index for the azimuth dependence
'e' : even azimuth dependence
'o' : odd azimuth dependence
'm' : order of solution in the azimuth direction
'n' : order of solution in the colatitude direction
z_n is a spherical Bessel function of type one, two or three and order n
P_n^m is the associated Legendre Polynomial of order (n, m).

It is now possible to write the solution to the time harmonic elastic wave equation as an infinite series

$$\begin{aligned}\vec{u}(r,\theta,\phi) = &\sum_{n=0}^{\infty} \sum_{m=0}^{n} \sum_{\sigma=e}^{o} a_{\sigma,m,n} \vec{L}_{\sigma,m,n}(k_p, r, \theta, \phi) + \\ &\sum_{n=0}^{\infty} \sum_{m=0}^{n} \sum_{\sigma=e}^{o} b_{\sigma,m,n} \vec{M}_{\sigma,m,n}(k_s, r, \theta, \phi) + \\ &\sum_{n=0}^{\infty} \sum_{m=0}^{n} \sum_{\sigma=e}^{o} c_{\sigma,m,n} \vec{N}_{\sigma,m,n}(k_s, r, \theta, \phi)\end{aligned} \quad (12)$$

with the vector functions $\vec{L}$, $\vec{M}$ and $\vec{N}$ as defined above.

The spherical vector functions $\vec{L}$, $\vec{M}$ and $\vec{N}$ can easily be implemented on a computer. If the coefficients $a_{\sigma,m,n}$, $b_{\sigma,m,n}$ and $c_{\sigma,m,n}$ in expansion (12) are known for a given elastic wave scattering problem, the displacement vector $\vec{u}$ can be computed everywhere. It is, for example, possible to expand a vectorial plane wave of arbitrary polarisation. In this case the coefficients can be determined analytically [3]. An expansion of stress components associated with elastic wave motion can also be written down. Its form is equivalent to (12), details can be found in [5]. For numerical reasons the infinite series (12) has to be truncated.

In order to study the scattering process from an indentation in an elastic half space with stress-free surface along the x axis the problem is split into two parts. The total displacement can be regarded as the displacement from an ideal elastic half-space with superimposed components representing the scattering object

$$\vec{u}_{total} = \vec{u}_{halfsp} + \vec{u}_{scatter} \quad (13)$$

The reflection of elastic plane waves from a plane stress-free surface is a straightforward algebraic problem, and the displacement and stress components for incident waves with arbitrary polarisation are easily determined.

The elastic displacement and stress components due to the scattering object are assumed as given through the expansion (12) with unknown coefficients $a_{\sigma,m,n}$, $b_{\sigma,m,n}$

and $c_{\sigma, m, n}$. The coefficients are now determined with the following method (point matching or collocation method) : Along the surface of the perturbed half space the normal stress components have to vanish, this is the definition of a stress-free surface. In order to achieve this, the normal stress components due to both the half space and the scattering object are computed along the surface of the perturbed half space at regular intervals, see Fig. 2. The sum of each normal stress component due to the half space plus the corresponding stress component due to the scatterer has to be zero at the sampling points (as ideally it should be everywhere on the surface) :

$$\underline{\sigma}_{total}\Big|_{s_i} \cdot \vec{n} = \left[\underline{\sigma}_{halfsp}\Big|_{s_i} + \underline{\sigma}_{scatter}\Big|_{s_i}\right] \cdot \vec{n} = 0 \qquad (14)$$

where $\vec{n}$ is the normal to the surface and s_i is a sampling point on the surface. If the number of sampling points is equal to the number of unknown coefficients in the expansion for the scattered field, a system of linear equations results which determines the coefficients. It is possible to do better by choosing the number of sampling points much greater than the number of unknown coefficients in the expansion. The coefficients can then be determined via a least squares method, i.e. minimising the error residual at the sampling points.

The surface perturbation is axisymmetric with respect to the z axis and is therefore independent of the azimuth coordinate ϕ. This allows a Fourier expansion of the incident and scattered wave fields with respect to the (spatial) variable ϕ in the interval $[0, 2\pi]$ and individual treatment of each Fourier component with subsequent superposition.

RESULTS

The computer program was checked against published results for the near-field displacements [2, 6] and gives excellent agreement. The results shown here were obtained for a hemispherical surface indentation in a half-space made of aluminium (ν= 0.34). Fig. 3 shows the surface displacements in the vicinity of the surface disturbance for a compressional plane wave incident at 60 degrees with the wave vector located in the x-z plane. The diameter of the hemisphere is half of a compressional wavelength. From the far-field radiation plots for the same case in Fig. 4 it can be seen that some energy is reflected back into the bulk material, but most of the energy is mode-converted into a Rayleigh wave. The amplitude of this surface wave is largest in the direction of the incident wave. Fig. 5 gives the far-field displacements for a hemispherical surface obstacle with a diameter of one compressional wavelength and all other parameters as before. The maximum in Fig. 5 is 3.88 times the maximum of Fig. 4. It can clearly be seen that very little energy is now scattered back into the bulk of the material and virtually all the scattered energy is converted into a Rayleigh wave travelling along the surface in the direction of incidence.

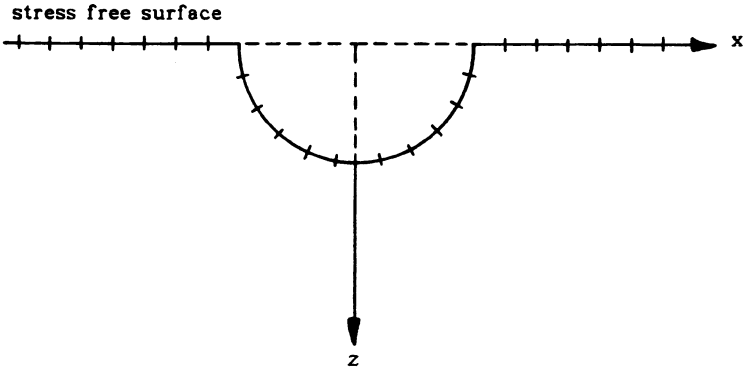

Fig. 2 . Sampling path indicating the collocation points in the x-z plane

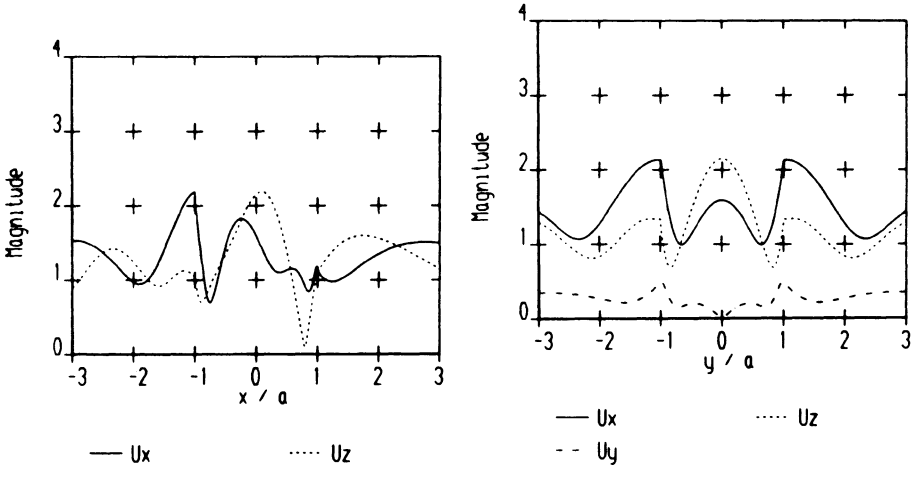

Fig. 3 . Surface displacements for a P wave incident on to a hemispherical surface disturbance at 60 degrees and $2a / \lambda_p = 0.5$. Thirteen basis functions were used in the expansion. Left : x-z plane, right : y-z plane.

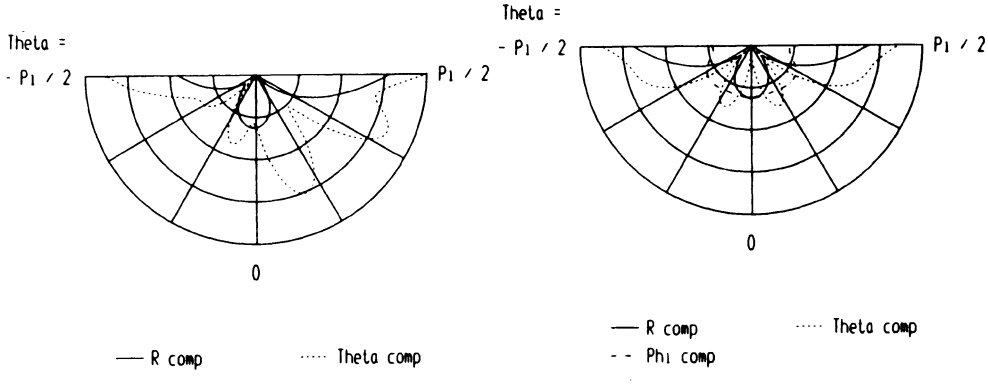

Fig. 4 . Far field displacements for a P wave incident on to a hemispherical surface disturbance at 60 degrees and $2a / \lambda_p = 0.5$. Thirteen basis functions were used in the expansion. Left : x-z plane, right : y-z plane.

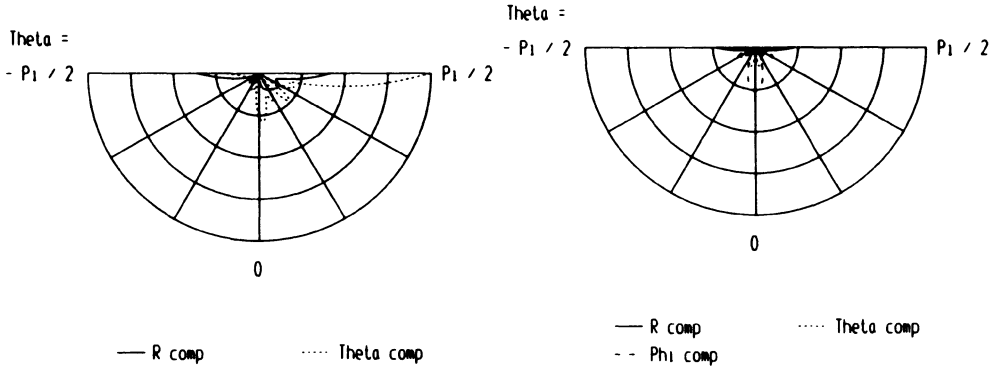

Fig. 5 . Far field displacements for a P wave incident on to a hemispherical surface disturbance at 60 degrees and $2a / \lambda_p = 1.0$. Sixteen basis functions were used in the expansion. Left : x-z plane, right : y-z plane.

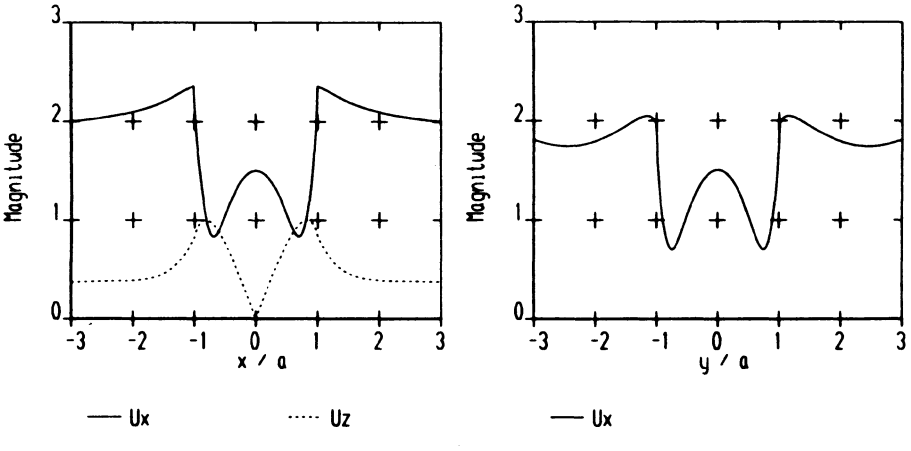

Fig. 6 . Surface displacements for a SV wave normally incident on to a hemispherical surface disturbance and $2a / \lambda_{sv} = 0.5$. Eleven basis functions were used in the expansion. Left : x-z plane, right : y-z plane.

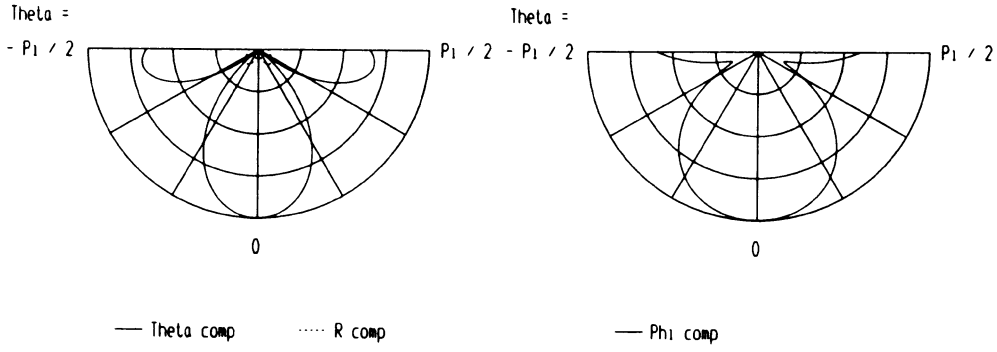

Fig. 7 . Far Field displacements for a SV wave normally incident on to a hemispherical surface disturbance and $2a / \lambda_{sv} = 0.5$. Eleven basis functions were used in the expansion. Left : x-z plane, right : y-z plane.

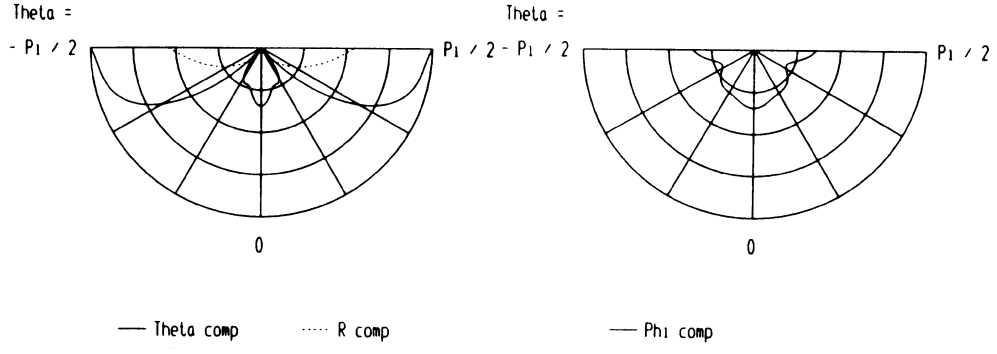

Fig. 8 . Far field displacements for a SV wave normally incident on to a hemispherical surface disturbance $2a / \lambda_{sv} = 1.0$. Thirteen basis functions were used in the expansion. Left : x-z plane, right : y-z plane.

The results shown in Fig. 6 to Fig. 8 lead to similar conclusions for the case of a shear wave normally incident on to the hemispherical surface disturbance. The maximum in Fig. 8 is 1.78 times the maximum of the previous plot. The wave components scattered into the bulk material appear to be stronger due to the normalisation with respect to the incident wavelength (here the shear wavelength). An interesting observation is that in the far field the scattered S wave components (Theta and Phi components) are stronger than the scattered P wave component (R component) for an incident SV wave as well as for an incident P wave. Due to the finite number of spherical vector functions employed to represent the scattered field it is impossible to model a Rayleigh wave accurately. This is only possible with an infinite number of vector functions. However, by including surface wave terms explicitly in (12) a proper account of surface waves should easily be possible.

CONCLUSIONS

The results obtained with the boundary method presented above demonstrate its effectiveness for simulating three-dimensional elastic wave scattering from indented plane stress-free surfaces. The ratio of diameter of the surface disturbance to incident wavelength can vary from $2a/\lambda = 0.25$ up to $2a/\lambda = 2.0$, and far-field radiation diagrams as well as plots of the surface movements in the vicinity of the indentation can be generated. The shape of the surface disturbance is not restricted to hemispherical obstacles, work carried out on the scattering from non-hemispherical axisymmetric surface features is reported in [7].

ACKNOWLEDGEMENT

This work was performed with the support of the Procurement Executive of the Ministry of Defence and the Department of Trade and Industry, UK. Peter Albach would like to thank Prof. J. Brian Davies from University College London and Dr David Bruce from RAE Farnborough, UK, for their help and advice.

REFERENCES

1. R. E. Beissner and A. S. Birring, Nondestructive Evaluation Methods for Characterizeration of Corrosion, State of the Art Review, Nondestructive Testing Information Analysis Center, Southwest Research Institute, San Antonio, Texas, December 1988
2. Francisco J. Sanchez-Sesma, Diffraction of Elastic Waves by Three-Dimensional Surface Irregularities, Bull. Seism. Soc. Am., 73, pp 1621 - 1636, December 1983
3. Philip M. Morse and Herman Feshbach, Methods of Theoretical Physics, Part II, McGraw-Hill Book Company, New York, Toronto, London, 1953
4. Charles L. Lawson and Richard J Hanson, Solving Least Squares Problems, Prentice-Hall, Inc., Englewood Cliffs, New Jersey, 1974
5. Yih-Hsing Pao and Chao-Chow Mow, Diffraction of Elastic Waves and Dynamic Stress Concentration, Adam Hilger Ltd, London, 1973
6. Fransico J. Sanchez-Sesma, Site effects on strong ground motion, Soil Dynamics and Earthquake Engineering, 6, pp 124 - 132, 1987
7. Peter H. Albach and Leonard J. Bond, Three-Dimensional Numerical Simulation of Elastic Body Waves Scattered from a Half-Space with Hemispherical or Shallow Surface Indentations, Proceedings of the IUTAM Symposium on Elastic Wave Propagation and Ultrasonic NDE, Elsevier Science Publishers, (to be published)